Dephasing Time in Graphene Due to Interaction with Flexural Phonons

Konstantin S. Tikhonov,[1,2,3,4,†] Wei L. Z. Zhao,[1,2,*] and Alexander M. Finkel'stein[1,2,5]
[1]Department of Physics and Astronomy, Texas A&M University, College Station, Texas 77843-4242, USA
[2]Department of Condensed Matter Physics, The Weizmann Institute of Science, 76100 Rehovot, Israel
[3]L. D. Landau Institute for Theoretical Physics, 117940 Moscow, Russia
[4]Moscow Institute of Physics and Technology, 141700 Moscow, Russia
[5]Institut für Nanotechnolsogie, Karlsruhe Institute of Technology, 76021 Karlsruhe, Germany
(Received 19 May 2014; published 13 August 2014)

We investigate decoherence of an electron in graphene caused by electron-flexural phonon interaction. We find out that flexural phonons can produce a dephasing rate comparable to the electron-electron one. The problem appears to be quite special because there is a large interval of temperature where the dephasing induced by phonons cannot be obtained using the golden rule. We evaluate this rate for a wide range of density (n) and temperature (T) and determine several asymptotic regions with the temperature dependence crossing over from $\tau_\phi^{-1} \sim T^2$ to $\tau_\phi^{-1} \sim T$ when temperature increases. We also find τ_ϕ^{-1} to be a nonmonotonic function of n. These distinctive features of the new contribution can provide an effective way to identify flexural phonons in graphene through the electronic transport by measuring the weak-localization corrections in magnetoresistance.

DOI: 10.1103/PhysRevLett.113.076601 PACS numbers: 72.80.Vp, 72.10.Di

Introduction.—The transport properties of graphene have attracted much attention [1] since the first discovery of this fascinating material [2]. It is promising for various applications due to its high charge mobility and unique heat conductivity. Theoretically, it was realized long ago [3–5] that these transport properties of free-standing (suspended) graphene are strongly influenced by flexural (out-of-plane) vibrational modes that deform the graphene sheet. From the experimental point of view, the effect of flexural phonons (FPs) was clearly observed in heat transport [6,7]. However, it is a more challenging task to identify the effect of flexural phonons in electronic transport [8,9]. This is because the contribution of electron-phonon interactions to momentum relaxation remains small even at high temperatures, with the main source of the relaxation being elastic impurities [10].

The dephasing rate τ_ϕ^{-1}, on the other hand, is a more suitable quantity for studying FPs, since static impurities do not cause dephasing. Usually, electron-electron interactions [11–15] are considered the primary mechanism for dephasing. In this Letter, we discuss dephasing caused by the electron-flexural phonon (el-FP) interaction in graphene. It is the softness of the flexural mode and the coupling of an electron to two FPs simultaneously (see Fig. 1 for illustration) that make the contribution of FPs to τ_ϕ^{-1} significant in a suspended sample, and at large enough densities comparable with the one caused by the electron-electron interaction. Because of the quadratic spectrum of FPs, $\omega_k = \alpha k^2$, they are much more populated as compared with in-plane phonons. In addition, the coupling to two FPs considerably increases the phase space available for inelastic processes as compared to the interaction with a single phonon. The point is that in graphene the Fermi momentum k_F is relatively small. As a result, the interaction of a single phonon with electrons is determined by the Bloch-Grüneisen temperature, $T_{\mathrm{BG}} \sim \omega_{2k_F}$, rather than the temperature, when $T \gg T_{\mathrm{BG}}$ [16]. In such a case, one needs to exploit other scattering mechanisms to overcome the limitations induced by the smallness of k_F [17]. In the case of el-FP interaction, coupling to two phonons radically changes the situation. Now only the transferred momentum should be small, while individually a FP may have a momentum much larger than k_F, up to the thermal momentum q_T.

Still, as we shall demonstrate, the problem of dephasing due to the el-FP interaction appears to be quite special, because the softness of FPs, i.e., the unique smallness of T_{BG}, leads to the existence of a temperature range where dephasing rate cannot be obtained using the golden rule (GR). Rather, both the self-energy and the vertex processes

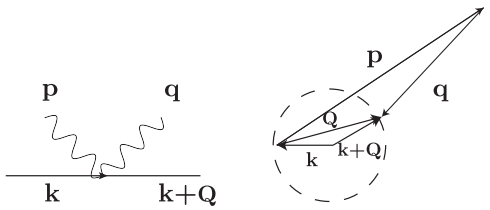

FIG. 1. On the left: Scheme of the el-FP interaction process, where the solid line represents an electron, and the wavy lines represent FPs. On the right: FPs can have momenta **p**, **q** much larger than the transferred momentum **Q**. Under the conditions discussed in the Letter, the scattering process is considered as semielastic.

[18] should be treated simultaneously. This results in a transition from $\tau_\phi^{-1} \sim T^2$ to T with increasing temperature for the dephasing rate induced by FPs.

The electron-flexural phonon interaction.—Lattice dynamics of the single-layer graphene can be described in terms of the displacement vector $\mathbf{u} = (u_x, u_y, h)$ [19]. Here $u_{x,y}$ describe the in-plane modes, while the out-of-plane displacement h describes the flexural mode. The displacement vector leads to a nonlinear strain tensor $u_{ij} = \frac{1}{2}(\partial_i u_j + \partial_j u_i + \partial_i h \partial_j h)$, where $(i,j) = (x,y)$ are spatial indices. The lattice modes interact with electrons through emergent scalar and vector potential fields [20,21]:

$$\varphi = g_1(u_{xx} + u_{yy}),$$
$$\mathbf{A}^\alpha = s^\alpha g_2/v_F(u_{xx} - u_{yy}, -2u_{xy}), \tag{1}$$

where $g_1 = 30$ eV, $g_2 = 7.5$ eV [9], and v_F is the Fermi velocity. Index $\alpha = K, K'$ describes two valleys of the conducting electron band, and factor $s^{K/K'} = \pm 1$ reflects the fact that the emergent vector potential $\mathbf{A}^\alpha$ respects the time reversal symmetry.

Thermal fluctuations of the lattice produce variations in the potentials. Averaging over lattice vibrations one finds the correlation functions of the potentials as

$$\langle \varphi(\mathbf{Q},\Omega)\varphi(-\mathbf{Q},-\Omega)\rangle = \phi(\mathbf{Q},\Omega),$$
$$\langle A_i^\alpha(\mathbf{Q},\Omega)A_j^\beta(-\mathbf{Q},-\Omega)\rangle = s^\alpha s^\beta \mathcal{A}_{ij}(\mathbf{Q},\Omega). \tag{2}$$

To proceed, we introduce the correlation function for FP

$$\langle h(\mathbf{k},\omega)h(-\mathbf{k},-\omega)\rangle \equiv H(k)2\pi\delta(\omega - \omega_k), \tag{3}$$

where $H(k) = (n(\omega_k)/\rho\omega_k)$. In this equation, $n(\omega)$ is the Planck distribution function and ρ is the mass density of the graphene sheet. One can propose the following form of the spectrum of the flexural phonon:

$$\omega_k = \alpha k^2 \Theta(k), \qquad \Theta(k) = \sqrt{1 + Z^{-1}(q_c/k)^\eta}, \tag{4}$$

where $\Theta(k)$ describes a transition from the bare spectrum at high momentum to the renormalized spectrum $\sim k^{2-\eta/2}$ in the low momentum limit. At $k < q_c(T) = (\sqrt{T\Delta_c}/v_F)$ the quadratic spectrum for the flexural mode ceases to work due to anharmonicity. Here $\Delta_c \approx 18.7$ eV [5] reflects the energy scale of anharmonicity. The anharmonicity is related to the h^4 vertex, arising as a result of integrating out fast u modes, which are coupled to the h mode [22]. Below we will exploit the value $Z \sim 2$, and take $\eta \approx 0.8$ from the numerical solution of the self-consistent screening approximation theory [23,24].

We consider graphene away from the Dirac point at chemical potential $\mu \gg T$. Besides k_F, the relevant momentum scales in the problem are thermal momentum $q_T = \sqrt{T/\alpha} \approx 0.05\sqrt{T[\mathrm{K}]}/\text{Å}$ and $q_c(T) \approx 0.01\sqrt{T[\mathrm{K}]}/\text{Å}$, which signals the transition to the renormalized FP spectrum. From now on, we will concentrate on the realistic situation from the experimental viewpoint: $k_F \ll q_T$, i.e., $T \gg T_{\mathrm{BG}}$. The Bloch-Grüneisen temperature $T_{\mathrm{BG}} = \omega_{2k_F} \approx 0.4\Theta(2k_F)$ nK, where n is the electronic density measured in units of 10^{12} cm^{-2}. Note T_{BG} is extraordinarily small for all relevant densities. As we have already emphasized, see Fig. 1, the momentum transfer in the el-FP interaction is limited by $2k_F$. Nevertheless, the extended structure of the correlation functions $\phi(\mathbf{Q},\Omega)$ and $\mathcal{A}_{ij}(\mathbf{Q},\Omega)$ enables electrons to have energy transfer exceeding the phonon energy ω_{2k_F}.

The main tool to probe electronic coherence is magnetoresistance [25], which gives a direct access to the weak-localization corrections to conductivity, controlled by the dephasing rate τ_ϕ^{-1}. The weak-localization correction to conductivity in graphene can be written as [26,27]

$$\Delta\sigma = -\frac{2e^2 D}{\pi}\sum_l \int dt C^l(-t/2, t/2), \tag{5}$$

where l sums over four Cooperon channels relevant for the magnetoresistance. Physically, $C^l(-t/2,t/2)$ represents the interference of a pair of time reversed trajectories in the channel l that start at $-t/2$ and return to the initial point at $t/2$. More generally, the Cooperon matrix $C^{l_1 l_2}_{s_1 s_2}$ is labeled by two isospin numbers $s_{1,2}$ and two pseudospin numbers $l_{1,2}$. This matrix is diagonal in the pseudospin space even in the presence of interactions that preserve sublattice and valley indices. The Cooperon channels relevant for magnetoresistance are the isospin singlets, $C^l \equiv C^{ll}_{00}$ $(l = 0, x, y, z)$, that do not have gaps comparable with τ^{-1}, the elastic scattering rate due to impurities. Therefore, we restrict ourselves to this subspace.

To include el-FP interaction into the Cooperon, one can write down a Bethe-Salpeter equation for a particular Cooperon channel C^l; see Fig. 2. In the following we will not solve the equation exactly, but instead, we will estimate the upper bound of the Cooperon decay rate [28,29]. We start by writing down an ansatz that reads as [18]

$$C^l(t_1,t_2) = C_0^l(t_1 - t_2)e^{-F^l(t_1,t_2)}. \tag{6}$$

Here $C_0^l(t)$ is the diffusion propagator describing the bare Cooperon, and $F^l(t_1,t_2)$ is a decay function characterizing the effect of the el-FP interaction [30].

Dephasing due to scalar potential fluctuations.—For the scalar potential correlation function one obtains

$$\phi(\mathbf{Q},\Omega) = \frac{1}{8}g_1^2(Q)\int (d^2\mathbf{p})(d^2\mathbf{q})[\mathbf{p}\cdot\mathbf{q}]^2 \times H(p)H(q)\delta_{\mathbf{p},\mathbf{q}}(\Omega,\mathbf{Q}), \tag{7}$$

where $\delta_{\mathbf{p},\mathbf{q}}(\Omega,\mathbf{Q}) \equiv \sum_\pm (2\pi)^3\delta(\Omega \pm \omega_{\mathbf{p}} \pm \omega_{\mathbf{q}}) \times \delta(\mathbf{Q} - \mathbf{p} - \mathbf{q})$, and $\omega_{\mathbf{p},\mathbf{q}}$ are given by Eq. (4). Here summation includes

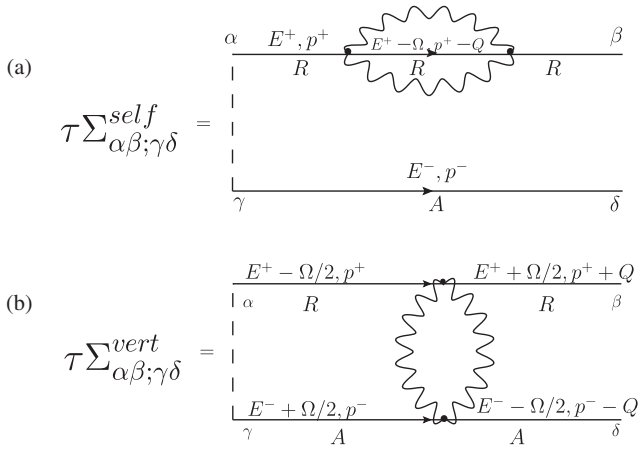

FIG. 2. Diagrammatic representation of (a) the self-energy and (b) the vertex FP contribution to the Cooperon; see also Fig. 2(c) in [30].

four different processes of emission or absorption of two FPs by an electron. The screened coupling constant $g_1(Q) = g_1(Q/Q + \varkappa)$, where $\varkappa = g_e N k_F$, $N = 4$ is the spin-valley degeneracy in graphene, and $g_e \sim 1$ describes the renormalized Coulomb interaction [33]. Since each time an electron is coupled to *two* flexural phonons, ϕ describes a phonon loop and, therefore, in the momentum-frequency domain $\phi(\mathbf{Q}, \Omega)$ has an extended support rather than a δ-function peak. As a result, the decay function for the scalar potential $F_\phi(t)$ (which is the same for all channels) can be expressed as a convolution of the three factors [30]: (i) the correlation function $\phi(\mathbf{Q}, \Omega)$, (ii) function $\mathcal{B}_\phi(\mathbf{Q})$, describing the ballistic electron's motion, and (iii) factor $\mathcal{C}^\phi(\Omega, t)$, reflecting the relation between the self-energy and vertex diagrams:

$$F_\phi(t) = t \int (d\mathbf{Q})(d\Omega)\phi(\mathbf{Q}, \Omega)\mathcal{B}_\phi(\mathbf{Q})\mathcal{C}^\phi(\Omega, t). \quad (8)$$

Here,

$$\mathcal{B}_\phi(\mathbf{Q}) = \frac{2}{v_F Q}(1 - (Q/2k_F)^2)^{1/2}\theta(2k_F - Q), \quad (9)$$

where the Heaviside theta function $\theta(2k_F - Q)$ restricts momentum that can be exchanged between FPs and electrons. The factor $\mathcal{C}^\phi(\Omega, t)$ is equal to

$$\mathcal{C}^\phi(\Omega, t) = 1 - \frac{\sin \Omega t}{\Omega t}, \quad (10)$$

and it describes the balance between the self-energy and vertex diagrams on Fig. 2. $\mathcal{C}^\phi$ is sensitive to the dynamic aspect of the scattering event and, because of this, alters the temperature dependence of τ_ϕ^{-1}.

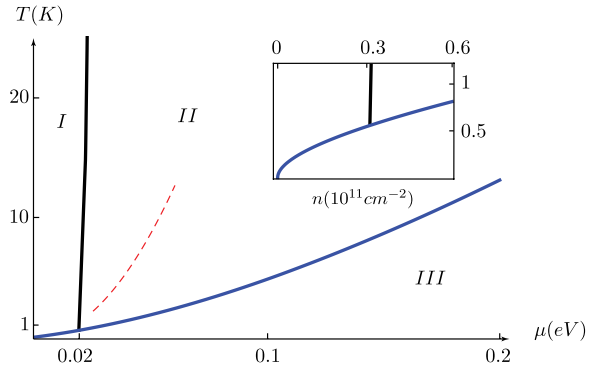

FIG. 3 (color online). Phase diagram of the dephasing rate due to FPs with scalar coupling. The blue and black lines divide the whole $(T - \mu)$ plane into three regions; see the text for explanations. The blue line coincides with the maximum of the dephasing rate as a function of chemical potential at a fixed temperature; see Fig. (4). The red dashed line representing a fragment of $\xi = 1$ is shown here for orientation. The inset is a zoom in of the intersection area of the blue and black lines plotted as a function of the electronic density.

The dephasing rate τ_ϕ^{-1} is defined according to $F_\phi(\tau_\phi) = 1$. The decay function can be most conveniently expressed as

$$F_\phi(t) = c_\phi^2 t T f(\mathcal{T}, \xi)\frac{T}{\mu}, \quad (11)$$

where $c_\phi = (g_1/\rho\alpha^2/2\pi g_e N) \sim 1.2$ is a dimensionless coupling constant and f is a dimensionless function of two parameters: $\mathcal{T} = \alpha k_F^2 t$ and $\xi = Z^{-1/\eta} q_c/k_F$ [30]. Parameter ξ originates from the renormalization of the FP spectrum described by Θ in Eq. (4); $\Theta(k_F) = \sqrt{1 + \xi^\eta}$. At small $\mathcal{T}$ the function f is linear in $\mathcal{T}$, and it saturates at $\mathcal{T} \gg 1$.

The results are illustrated with the help of Fig. 3, where regions I, II, and III with a different dephasing rate behavior are indicated in the $(T - \mu)$ plane. The regions are divided in accord with the importance of the renormalized spectrum of the FP and the relative contributions of the self-energy and vertex diagrams. In region I, which is on the left of the black line (i.e., at small densities), the characteristic momenta of p and q in Eq. (7) do not exceed q_c. Therefore, the renormalization of the FP spectrum is important, and $\omega_q \sim q^{2-\eta/2}$ should be used [34]. In region II, since the characteristic momenta of the FPs are larger than q_c, it suffices to use the quadratic spectrum for FPs. In region III, which is in the bottom part below the blue line, the dephasing time is long and only the self-energy diagram is important. Hence, the factor $\mathcal{C}^\phi$ reduces to 1, and the dephasing rate coincides with the out-scattering rate τ_{out}^{-1} obtained from the golden rule [5]. (In this calculation, q_c just provides an infrared cutoff.) Above the blue line, in regions I and II, both the self-energy and vertical diagrams

are relevant, and the factor $\mathcal{C}^{\phi}(t)$ is important; see also [35]. Because of the two-phonon structure of the correlation function of the FP pairs participating in the inelastic process, the influence of this factor on the dephasing rate is rather nontrivial, so that one cannot expand $\mathcal{C}^{\phi}(t)$.

In Fig. 3, the blue and black lines have been found by matching the asymptotic behavior [30] of the dephasing rates deep in regions I, II, and III. We introduce (μ_0, T_0) the values of the crossing point of the blue and black lines as characteristic scales: $\mu_0 \sim (\gamma/c_\phi^2)\Delta_c$ and $T_0 \sim (\gamma/c_\phi^2)\mu_0$. Here, we have introduced $\gamma = (\alpha\Delta_c/v_F^2) \sim 0.02$, which is a parameter describing the adiabaticity of the el-FP interaction. Under a given choice of parameters, it can be found numerically that $\mu_0 \approx 0.02$ eV and $T_0 \approx 0.6$ K. The dephasing rate in different regions can be expressed as

$$\tau_\phi^{-1}(T) = \gamma T \times \begin{cases} 0.48(\mu/\mu_0)^{(4-\eta/8-5\eta)} & \text{I} \\ 0.18\sqrt{\mu/\mu_0} & \text{II} \\ 0.24\frac{T/T_0}{\mu/\mu_0}\log\xi^{-1} & \text{III.} \end{cases} \quad (12)$$

These expressions are obtained using asymptotic behavior of the function f in Eq. (11) and, therefore, are only applicable far away from the borderlines. At low enough temperatures $\mathcal{C}^{\phi}(t) = 1$ and the function $f(\mathcal{T}, \xi)$ is independent of $\mathcal{T}$. Hence, $\tau_\phi^{-1} \sim T^2$ in region III, which is a GR result. At high temperatures the phonons contributing to the electronic dephasing become quasistatic and, consequently, the dephasing rate is smaller than the out-scattering rate τ_{out}^{-1}. Unlike region III, in regions I and II the dephasing rate is determined by a non-GR expression, and is proportional to temperature, irrespective of η. The existence of the linear in T regime is the main result of our Letter.

By comparing the rates in regions II and III, one may conclude that there should be a maximum in the dephasing rate as a function of μ. Indeed, as it is illustrated by Fig. 4 such a maximum exists. The line indicating the maximum essentially overlaps with the borderline between the regions I, II and the region III, which is illustrated by the blue line in Fig. 3.

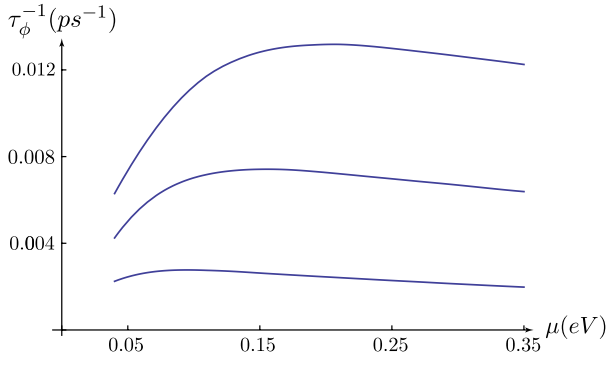

FIG. 4 (color online). Dephasing rate as a function of the chemical potential at different temperatures. From top to bottom: $T = 15, 10, 5$ K.

Dephasing due to vector potential fluctuations.—Unlike the scalar potential, the dephasing rates induced by vector potential are different for different channels owing to the factor $\mathcal{C}_l^A(\Omega, t) = 1 + s_l(\sin\omega t/\omega t)$, where $s_l = -1$ for the intervalley Cooperons $(l = 0, z)$ and $s_l = 1$ for the intravalley Cooperons $(l = x, y)$. For the magnetoresistance at weak fields, only the intervalley channels are important. The dephasing rate produced by the vector potential coupling is quite similar to its scalar counterpart, Eq. (12), with obvious modifications due to the change in the coupling constant and the absence of screening for the vector potential [30].

Discussion.—We have analyzed the dephasing rate induced by FPs in graphene, and evaluated it for a wide range of n and T (see Fig. 3). We determined several asymptotic regions with temperature dependence evolving from $\tau_\phi^{-1} \sim T^2$ to $\tau_\phi^{-1} \sim T$ when the temperature increases. (See Fig. 4 in [30] for an illustration of the temperature dependence of the dephasing rate.) The transition to linear behavior in T is related to the fact that at high temperatures phonons become slow on the time scale of τ_ϕ.

The measured dephasing rate in graphene is usually compared to the contribution induced by the electron-electron interaction, τ_{ee}^{-1}, which is linear in T for $T < 1/\tau_{tr}$ [11]. However, the observed rate [12–14], when it is linear in T, always exceeds the theoretical estimation. In view of the linear dependence on T of the FP's contribution to dephasing, it is reasonable to compare its value with τ_{ee}^{-1}. In principle, it is a competition between two mechanisms, each determined by a small parameter: the adiabatic parameter γ and sheet resistance $\rho_\square$ measured in units of the quantum resistance. We compare the dephasing rates at density $n = 10^{12}$ cm^{-2} when the sheet resistance $\approx 0.5k\Omega$. Under these conditions, both parameters γ and $\rho_\square$ are of the same value. Combining the contributions arising from the scalar and vector potentials, we obtain $\tau_{\text{FP}}^{-1}/\tau_{ee}^{-1} \approx 0.2$.

The in-plane phonons generate a dephasing τ_{in}^{-1} that at $T < T_{\text{BG}}^{\text{in}}$ is negligible compared with τ_{FP}^{-1}, while at $T > T_{\text{BG}}^{\text{in}}$ the rate $\tau_{\text{in}}^{-1} \sim T$ is comparable with τ_{FP}^{-1}. (Note that for in-plane phonons, a region of non-GR dephasing rate, analogous to region II, develops at temperatures $\gtrsim\mu$ that are too high to be relevant.) It is important that each of the three rates τ_{ee}^{-1}, τ_{FP}^{-1}, and τ_{in}^{-1}, has a distinct dependence on the chemical potential. While τ_{ee}^{-1} decreases with density, $\tau_{\text{FP}}^{-1} \propto \mu^{1/2}$ and $\tau_{\text{in}}^{-1} \propto \mu$. This opens a way to identify each of these mechanisms by studying the magnetoresistance as a function of the chemical potential.

In our consideration, we had in mind suspended graphene. However, our result may also be relevant for supported samples so long as they are coupled to the substrate by weak van der Waals forces [36]. One may expect that such a weak coupling does not provide an

essential change in the phonon spectrum. Indeed, it is known that the phonon spectrum in graphene [37] and graphite [38] is practically identical for the corresponding branches. FPs in supported samples have been discussed recently in connection with the heat transport measurements in Refs. [6,7]. Until now, flexural phonons have been a delicate object to detect in electronic transport. We propose here to observe them through weak-localization measurements.

The authors gratefully acknowledge A. Dmitriev, I. Gornyi, V. Kachorovskii, D. Khmelnitskii, and A. Mirlin for the useful discussions and valuable criticism. We thank Jonah Waissman for reading our manuscript. The authors thank the members of the Institut für Theorie der Kondensierten Materie at KIT for their kind hospitality. A. F. is supported by the Alexander von Humboldt Foundation. The work is supported by the Paul and Tina Gardner fund for the Weizmann-TAMU Collaboration, and National Science Foundation Grant No. NSF-DMR-100675. K. T. and W. Z. contributed equally to this work.

*Corresponding author.
wei.zhao@tamu.edu
†tikhonov@physics.tamu.edu

[1] S. Das Sarma, S. Adam, E. H. Hwang, and E. Rossi, Rev. Mod. Phys. **83**, 407 (2011).
[2] A. H. Castro Neto, N. M. R. Peres, K. S. Novoselov, and A. K. Geim, Rev. Mod. Phys. **81**, 109 (2009).
[3] E. Mariani and F. von Oppen, Phys. Rev. Lett. **100**, 076801 (2008).
[4] H. Ochoa, E. V. Castro, M. I. Katsnelson, and F. Guinea, Phys. Rev. B **83**, 235416 (2011).
[5] I. V. Gornyi, V. Y. Kachorovskii, and A. D. Mirlin, Phys. Rev. B **86**, 165413 (2012).
[6] A. A. Balandin, S. Ghosh, W. Bao, I. Calizo, D. Teweldebrhan, F. Miao, and C. N. Lau, Nano Lett. **8**, 902 (2008).
[7] J. H. Seol *et al.*, Science **328**, 213 (2010).
[8] K. I. Bolotin, K. J. Sikes, J. Hone, H. L. Stormer, and P. Kim, Phys. Rev. Lett. **101**, 096802 (2008).
[9] E. V. Castro, H. Ochoa, M. I. Katsnelson, R. V. Gorbachev, D. C. Elias, K. S. Novoselov, A. K. Geim, and F. Guinea, Phys. Rev. Lett. **105**, 266601 (2010).
[10] E. H. Hwang and S. Das Sarma, Phys. Rev. B **77**, 115449 (2008); note that the phonon's contribution to resistivity is about 100 Ohm on the background of few kOhms.
[11] B. L. Altshuler, A. G. Aronov, and D. E. Khmelnitsky, J. Phys. C **15**, 7367 (1982).
[12] X. Wu, X. Li, Z. Song, C. Berger, and W. A. de Heer, Phys. Rev. Lett. **98**, 136801 (2007).
[13] F. V. Tikhonenko, A. A. Kozikov, A. K. Savchenko, and R. V. Gorbachev, Phys. Rev. Lett. **103**, 226801 (2009).
[14] M. B. Lundeberg and J. A. Folk, Phys. Rev. Lett. **105**, 146804 (2010).
[15] J. Jobst, D. Waldmann, I. V. Gornyi, A. D. Mirlin, and H. B. Weber, Phys. Rev. Lett. **108**, 106601 (2012).
[16] D. K. Efetov and P. Kim, Phys. Rev. Lett. **105**, 256805 (2010).
[17] J. C. W. Song, M. Y. Reizer, and L. S. Levitov, Phys. Rev. Lett. **109**, 106602 (2012).
[18] J. von Delft, F. Marquardt, R. A. Smith, and V. Ambegaokar, Phys. Rev. B **76**, 195332 (2007).
[19] P. M. Chaikin and T. C. Lubensky, *Principles of Condensed Matter Physics*, Vol. 1 (Cambridge University Press, Cambridge, 2000).
[20] H. Suzuura and T. Ando, Phys. Rev. B **65**, 235412 (2002).
[21] J. L. Mañes, Phys. Rev. B **76**, 045430 (2007).
[22] D. R. Nelson and L. Peliti, J. Phys. (Paris) **48**, 1085 (1987).
[23] P. Le Doussal and L. Radzihovsky, Phys. Rev. Lett. **69**, 1209 (1992).
[24] K. V. Zakharchenko, R. Roldan, A. Fasolino, and M. I. Katsnelson, Phys. Rev. B **82**, 125435 (2010).
[25] B. L. Altshuler, D. Khmelnitzkii, A. I. Larkin, and P. A. Lee, Phys. Rev. B **22**, 5142 (1980).
[26] B. L. Altshuler, A. G. Aronov, and D. E. Khmelnitsky, Solid State Commun. **39**, 619 (1981).
[27] E. McCann, K. Kechedzhi, V. I. Fal'ko, H. Suzuura, T. Ando, and B. L. Altshuler, Phys. Rev. Lett. **97**, 146805 (2006).
[28] W. Eiler, J. Low Temp. Phys. **56**, 481 (1984).
[29] F. Marquardt, J. von Delft, R. A. Smith, and V. Ambegaokar, Phys. Rev. B **76**, 195331 (2007).
[30] See the Supplemental Material at http://link.aps.org/supplemental/10.1103/PhysRevLett.113.076601 for the diagrammatic calculation, evaluation, and asymptotic properties of the decay function, which includes Refs. [31,32].
[31] A. G. Aronov, A. D. Mirlin, and P. Wölfle, Phys. Rev. B **49**, 16609 (1994).
[32] A. G. Aronov and P. Wölfle, Phys. Rev. B **50**, 16574 (1994).
[33] V. N. Kotov, B. Uchoa, V. M. Pereira, F. Guinea, and A. H. Castro Neto, Rev. Mod. Phys. **84**, 1067 (2012).
[34] We, however, neglect the h^4-vertex corrections.
[35] G. Montambaux and E. Akkermans, Phys. Rev. Lett. **95**, 016403 (2005).
[36] A. K. Geim and I. V. Grigorieva, Nature (London) **499**, 419 (2013).
[37] D. L. Nika, E. P. Pokatilov, A. S. Askerov, and A. A. Balandin, Phys. Rev. B **79**, 155413 (2009).
[38] R. Al-Jishi and G. Dresselhaus, Phys. Rev. B **26**, 4514 (1982).